Bulletin of the Seismological Society of America, Vol. 97, No. 1A, pp. S192–S207, January 2007, doi: 10.1785/0120050613

Tsunami Source of the 2004 Sumatra–Andaman Earthquake Inferred from Tide Gauge and Satellite Data

by Yushiro Fujii* and Kenji Satake

Abstract Tsunami source of the 2004 Sumatra–Andaman earthquake was estimated from a joint inversion of tsunami waveforms recorded on tide gauges and sea surface heights captured by satellite altimetry measurements. The earthquake, the largest in the past 40 years, caused devastating tsunami damage to countries around the Indian Ocean, but the tsunami source, in particular, its northern end, was not well resolved. Although aftershocks and crustal deformation extended from off northwestern Sumatra Island through the Nicobar Islands to the Andaman Islands, some seismic-wave analyses indicated a shorter source length, several hundred kilometers. We used tsunami waveforms recorded at 12 tide gauge stations around the source and the sea surface heights measured by three satellites: Jason1, TOPEX/Poseidon, and Envisat. We numerically computed tsunami propagation using realistic bathymetry; more than 66,000 depth points were digitized from nautical charts and combined with the ETOPO2 data. Inversion of satellite data indicates that the tsunami source extended to the Andaman Islands with a total length of 1,400 km, but such a model produces much larger tsunami waveforms than observed at Indian tide gauge stations. Inversion of tide gauge records and the joint inversion indicate that the tsunami source was about 900 km long. The largest slip, about 13 to 25 m, was located off Sumatra Island and the second largest slip, up to 7 m, near the Nicobar Islands. The slip distribution is similar for different rupture velocities and rise times, with a slow velocity of 1 km/sec and a rise time of 3 min yielding the largest variance reduction.

Introduction

The Sumatra–Andaman earthquake (0:58:53 UTC, 26 December 2004) caused the worst tsunami damage in history; more than 200,000 people lost their lives in the countries around the Indian Ocean. The number of victims, both confirmed dead and missing, is largest in Indonesia (163,795), followed by Sri Lanka (35,399), India (16,389), and Thailand (8345) (International Federation of Red Cross and Red Crescent Societies, 2005). Within minutes of the earthquake, the tsunami devastated Banda Aceh and other coastal villages of Sumatra Island. The tsunami arrived at Thai, Sri Lankan, and Indian coasts about two hours after the earthquake. The tsunami propagated farther and arrived at the eastern coast of Africa several hours after the earthquake and caused 298 fatalities in Somalia. The tsunami was instrumentally recorded by coastal tide gauges around the Indian Ocean (Merrifield *et al.*, 2005; Nagarajan *et al.*, 2006). The tsunami propagation in the Indian Ocean was captured by satellite altimeters, probably for the first time (Gower, 2005).

The aftershock area extended from the epicenter off Sumatra through the Nicobar and Andaman Islands; the total length is about 1200 km. The estimated seismic-moment ranges from 4 to 10 $\times$ 10^{22} N m, or moment magnitude (M_w) between 9.0 and 9.3 (Park *et al.*, 2005; Stein and Okal, 2005), and made this event the largest in the world in the past 40 years. The rupture length, however, is controversial. Analysis of seismic body waves shows that, in part, because the time window for analysis is limited, the main moment release was limited to several hundred kilometers from the epicenter (Ammon *et al.*, 2005), whereas an array analysis indicated the rupture extended 1300 km (Ishii *et al.*, 2005). From arrival times of tsunamis, the major source of tsunami energy was estimated as 600–800 km long (Lay *et al.*, 2005b), though a later analysis indicated a longer source (Lay *et al.*, 2005a; Neetu *et al.*, 2005).

Tsunami source is seafloor deformation caused by slip on a fault during an earthquake. An important question about the 2004 earthquake is whether the tsunami source extended for 1200 km of the entire aftershock area. To estimate the

*Present address: International Institute of Seismology and Earthquake Engineering (IISEE), Building Research Institute (BRI), 1 Tachihara, Tsukuba, Ibaraki 305-0802, Japan.

tsunami source of the 2004 Sumatra–Andaman earthquake, we will use tsunami waveforms recorded on tide gauges and sea surface heights captured by satellite altimetry measurements. Tanioka *et al.* (2006) and Piatanesi and Lorito (2007) made inversion of tsunami waveform data, and Hirata *et al.* (2006) and Fine *et al.* (2005) used the satellite altimetry data. We first invert the waveform and satellite data separately, then perform the joint inversion of both data.

Data

Tide Gauge Data

The 2004 tsunami was recorded at more than 20 tide gauge stations around the source (Fig. 1). Some of them, namely in the Maldives and Sri Lanka (Colombo), have been collected by Global Sea Level Observing System (GLOSS) and were stored on the web site of University of Hawaii Sea Level Center (UHSLC) (Merrifield *et al.*, 2005). The Indian tide gauges are operated by Survey of India and the 2004 tsunami data were processed by National Institute of Oceanography (NIO) (Nagarajan *et al.*, 2006). The Indonesian tide gauge stations are operated by Geodesy and Geodynamic Center in Indonesia (GGCI) (Tanioka *et al.*, 2006). The tide gauges in Thailand are managed by Thai Marine Department (TMD) and Hydrographic Department, Royal Thai Navy (HDRTN) (Tsuji *et al.*, 2006). We downloaded digital data from the web sites or digitized the analog data (Table 1).

The tide gauge records usually include ocean tides. For the tsunami analysis, we need to separate the tsunami and tide signals. The UHSLC and NIO offered residual data, after the tidal component was removed. For the other data, we removed the tidal components by applying a high-pass filter.

The processed tide gauge records show clear tsunami signals (Fig. 2). The tsunami first-arrival times are about 120 min after the earthquake at Sibolga and Taphaonoi (Phuket), 140 min at Cocos, about 150 min on the east coast of India at Chennai, Vishakhapatnam, and Paradip, and larger at stations on the west coast of India, Maldives, and Thailand. The Port Blair record shows a gradual increase in sea level, which may indicate slow slip (Singh *et al.*, 2006), then was interrupted for 24 min (Neetu *et al.*, 2005); hence, we did not use this station for our analysis. Initial motion of tsunami was downward at stations east of the source (e.g., Taphaonoi or Tarutao) and upward at stations west of the source (e.g., Colombo or Male). Amplitudes of the initial tsunami wave range from several tens of centimeters to 2 m. The Colombo tide gauge record went off scale and is not usable after the first peak. The tsunami periods are typically longer than 20 min (Nagarajan *et al.*, 2006). These tsunami waveforms, or temporal changes of water height at tide gauge stations, will be used for inversion.

Satellite Altimeter Data

The tsunami wave field during propagation was captured by satellite altimeters as sea surface heights (SSHs) over the Indian Ocean. About 1.9 hr after the earthquake, satellite Jason-1 reached the wavefront of the tsunami and captured tsunami signals for 11 min of satellite transit time as it passed over the Indian Ocean from south to north (Gower, 2005). This altimetry measurement is numbered cycle 109 on pass 129. About 2 hr after the earthquake, satellite TOPEX/Poseidon flew over the ocean on a similar pass, which is numbered cycle 452 on pass 129. Later, about 3.2 hr after the earthquake, satellite Envisat flew from north to south over the ocean to capture the tsunami propagation. The cycle is numbered 33 on pass 352 (Fig. 3). We used altimetry data from these three satellites, Jason-1, TOPEX/Poseidon, and Envisat, downloaded from the Radar Altimeter Database System web site (http://rads.tudelft.nl/rads/data/authentication.shtml) by the Department of Earth Observation and Space Systems.

The observed SSH records include not only tsunami signals but also other oceanographic effects. To isolate tsunami signals, we used SSH data from previous cycles: 108 (16 December 2004) for Jason-1, 451 (16 December 2004) for TOPEX/Poseidon, and 32 (21 November 2004) for Envisat.

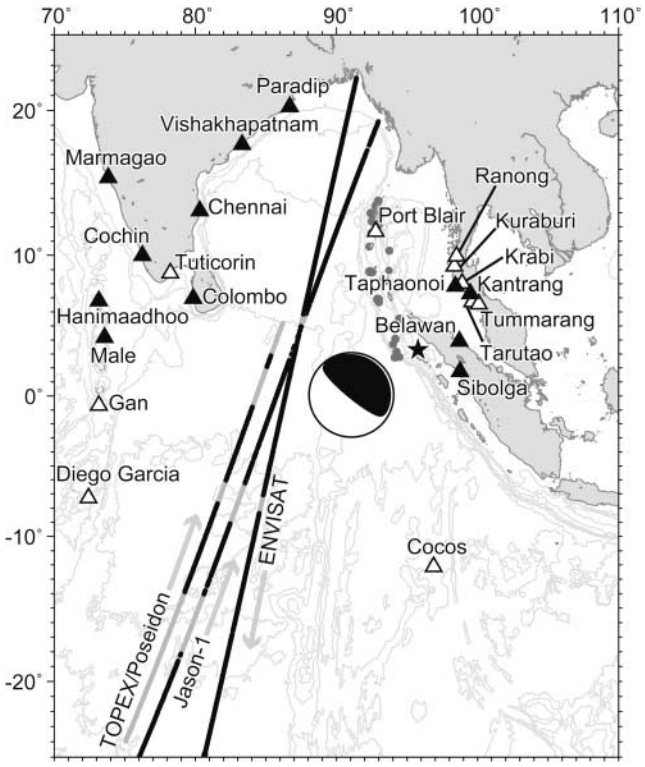

Figure 1. Epicenter of the 2004 mainshock (black star). Epicenters of aftershocks occurring one day after the mainshock (solid circles) located by the U.S. Geological Survey (USGS). Triangles indicate the location of available tide gauge stations; we used only the stations in black. The Harvard CMT solution is also shown (lower hemisphere equal-area projection). Track lines of three satellites (thick lines) are also shown.

Table 1
List of Tide Gauge Stations*

Station	Lat. (deg:min)	Lon. (deg:min)	D/A†	Agency‡	Source
Hanimaadhoo	6:46N	73:10E	2	UHSLC	Merrifield *et al.* (2005)§
Male	4:11N	73:32E	4	UHSLC	Merrifield *et al.* (2005)§
Gan	0:41S	73:09E	4	UHSLC	Merrifield *et al.* (2005)§
Diego Garcia	7:17S	72:24E	6	UHSLC	Merrifield *et al.* (2005)§
Colombo	6:57N	79:51E	2	UHSLC	Merrifield *et al.* (2005)§
Paradip	20:16N	86:42E	6	SOI	Nagarajan *et al.* (2006)
Vishakhapatnam	17:41N	83:17E	5‖	SOI	Nagarajan *et al.* (2006)
Chennai	13:06N	80:18E	5‖	SOI	Nagarajan *et al.* (2006)
Tuticorin	8:45N	78:12E	6	SOI	Nagarajan *et al.* (2006)
Cochin	9:58N	76:16E	6	SOI	Nagarajan *et al.* (2006)
Marmagao	15:25N	73:48E	5‖	SOI	Nagarajan *et al.* (2006)
Cocos	12:07S	96:53E	1	NTC	#
Port Blair	11:41S	92:46E	A	NIOT	Singh *et al.* (2006)
Sibolga	1:44N	98:48E	A	GGCI	Tanioka *et al.* (2006)
Belawan	3:55N	98:43E	A	GGCI	Tanioka *et al.* (2006)
Taphaonoi**	7:50.029N	98:25.274E	A	HDRTN	††
Tarutao‡‡	6:42:06N	99:39:00E	A	HDRTN	††
Kuraburi**	9:13.503N	98:22.613E	A	TMD	Tsuji *et al.* (2006)§§
Kantrang	—	—	A	TMD	Tsuji *et al.* (2006)§§
Krabi	—	—	A	TMD	Tsuji *et al.* (2006)§§
Ranong	—	—	A	TMD	Tsuji *et al.* (2006)§§
Tummarang	—	—	A	TMD	Tsuji *et al.* (2006)§§

*Location data of tide gauges are from Permanent Service for Mean Sea Level (PSMSL) web site, www.pol.ac.uk/psmsl/psmsl_individual_stations.html.
†D/A indicates sampling interval in minutes for digital data, A for analog data.
‡UHSLC, University of Hawaii Sea Level Center; SOI, Survey of India; NIOT, National Institute of Ocean Technology; GGCI, Geodesy and Geodynamic Center in Indonesia; TMD, Thai Marine Department; HDRTN, Hydrographic Department, Royal Thai Navy; NTC, National Tidal Centre, Australia.
§http://uhslc.soest.hawaii.edu/
‖Digitizing interval from analog data.
#www.bom.gov.au/info/tsunami/tsunami_info.shtml.
**Location data from Tsuji *et al.* (2006).
††www.navy.mi.th/hydro/tsunami.htm
‡‡Location data from www.navy.mi.th/hydro/tsunami.htm.
§§www.eri.u-tokyo.ac.jp/tsunami/thai_records/

Because the SSH locations on previous cycles may not be exactly the same as those during the tsunami, we have interpolated the SSH data of previous cycles by applying a moving average for 0.5 deg in latitude and resampling them to estimate the values at the same locations. Assuming that the other oceanographic effects are common to the both cycles, we consider that the difference between the two cycles, before and during the tsunami, represents the tsunami signal. The SSH data, or spatial distribution of tsunami water height with the satellite transit time considered, will be used for inversion.

The tsunami amplitude of the direct arrival in deep ocean is about 0.8 m. In SSH data of Jason-1, a broad peak appears at about 11° S in both cycles, before and after the tsunami. The narrow peaks at 5° S to 3° S appeared only after the tsunami; hence, we consider this as the tsunami signal. The TOPEX/Poseidon data show only a single peak. The Envisat data indicate many peaks in a wider area, because they captured the tsunami propagation at a later time.

Method

Fault Parameters

To estimate the extent of the tsunami source and the slip distribution, we divided the source into 22 subfaults that cover the aftershock area during one day after the mainshock (Fig. 4). The subfault size is 100 km × 100 km (Fig. 4 and Table 2). We fixed the size and geometry of each subfault and estimated the slip amount. This subfault geometry is similar to that of Hirata *et al.* (2006), who divided the source into 14 subfaults along the Sunda trench, but we further divided the southern eight subfaults into shallow and deep parts. The epicenter is located between the southernmost and next subfaults. The dip angle is assumed to be 10° from the aftershock distribution determined from ocean-bottom seismographic observation (Araki *et al.*, 2006), and the slip angles are based on the averaged compressional-axis directions of the aftershocks by the Harvard CMT catalog (Hirata *et al.*, 2006). Assuming that the rupture started from the epicenter and propagated unilaterally to the north at a constant veloc-

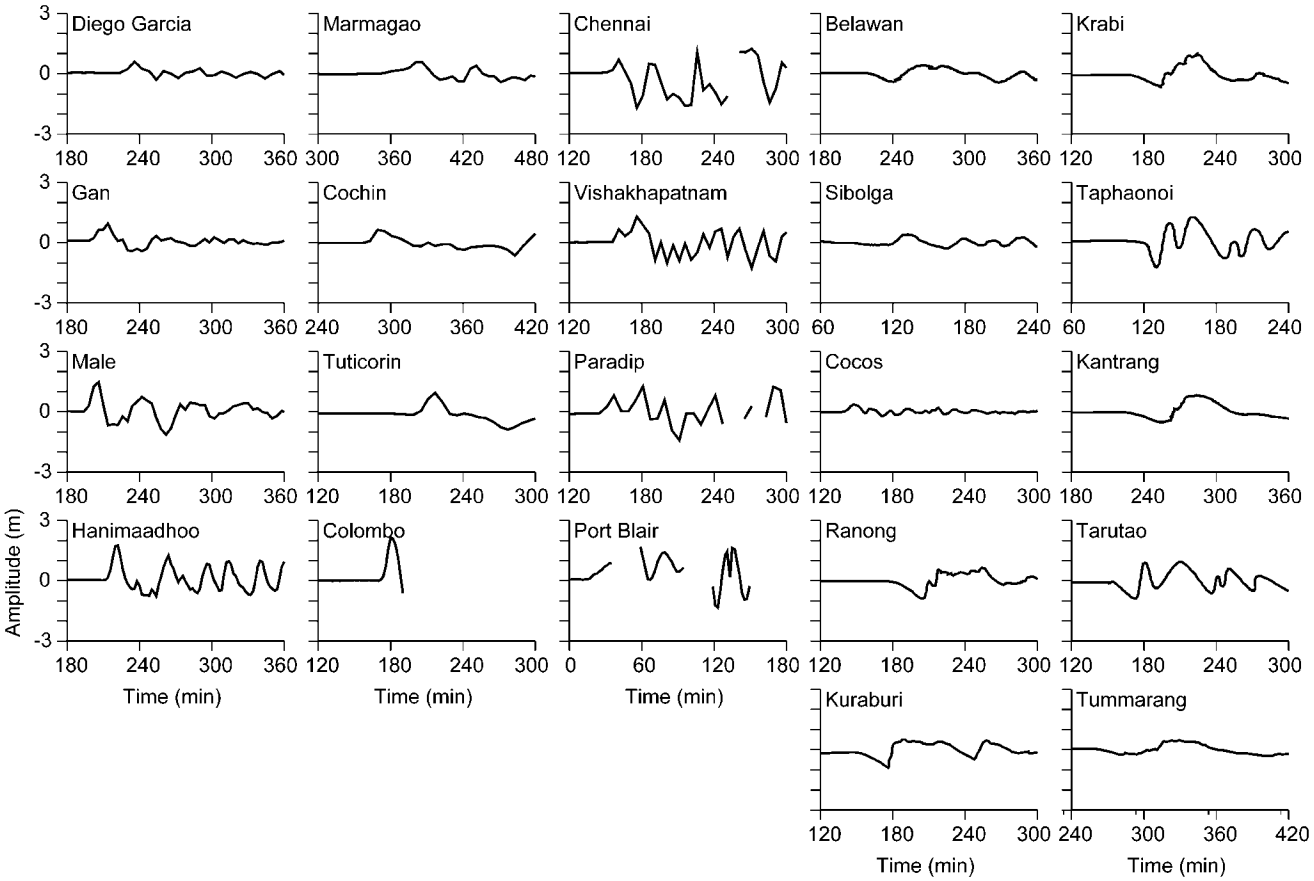

Figure 2. Tsunami waveforms at tide gauge stations. Time indicates the elapsed time (in minutes) from the earthquake origin time.

ity, we varied the rupture velocity from 0.5 to 3.0 km/sec at a 0.5 km/sec interval.

Finite-Difference Computation

To calculate tsunami propagation initiated at each subfault, the linear shallow-water long-wave equations were numerically solved by the finite-difference method (Satake, 1995). The equation of motion and the equation of continuity are written as

$$\frac{\partial V}{\partial t} = -g\nabla h \tag{1}$$

and

$$\frac{\partial h}{\partial t} = -d\nabla \cdot V, \tag{2}$$

respectively, where V is the depth-averaged horizontal velocity vector, h is the water elevation or tsunami amplitude, d is the water depth, and g is the gravitational acceleration. The computation area extends from 25° S to 25° N and 70° E to 110° E (Fig. 1). The bathymetric grid interval is basically 2 arc-minutes (about 3.7 km); hence, there are 1200 × 1500 grid points along the longitude and latitude directions, respectively. Near the coastal tide gauge stations, we used a finer grid interval of 24 arc-minutes (about 0.75 km) to better model near-shore propagation. A timestep of 2 sec is used to satisfy the stability condition for the finite-difference method. For the initial condition, static deformation of the seafloor was calculated by using the rectangular dislocation model (Okada, 1985). We also considered the effect of coseismic horizontal displacement in region of steep bathymetric slopes (Tanioka and Satake, 1996). Tsunami waveforms for tide gauge stations and SSH at observed points by satellites were calculated assuming a constant rise time (or slip duration) on each subfault of 1, 2, and 3 min. Because the subfault size is 100 km × 100 km, these assumed rise times include the effect of rupture propagation within each subfault.

Bathymetry Data

Because the phase speed of long waves depends only on the water depth, accurate bathymetric data are essential

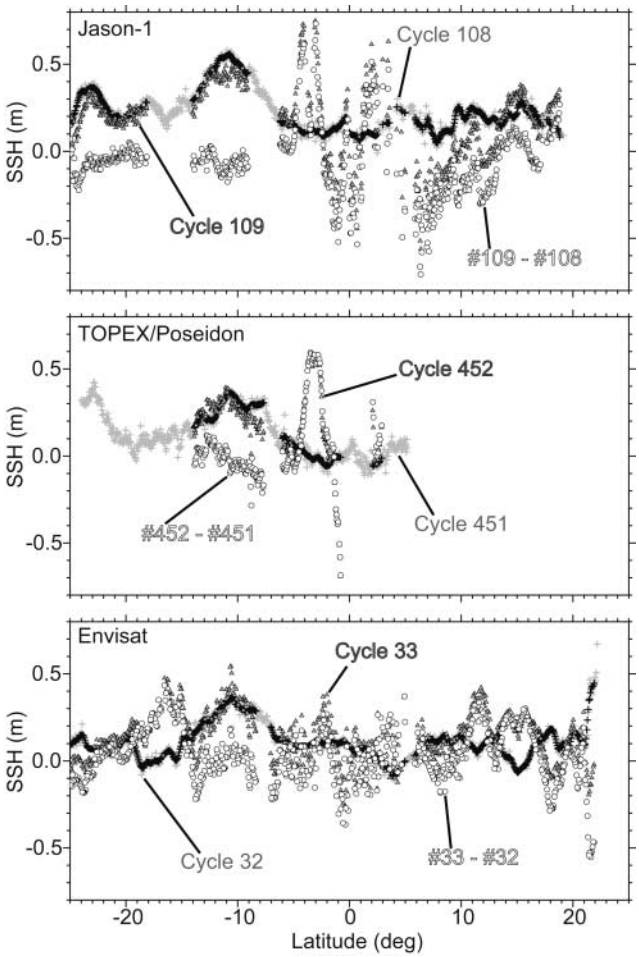

Figure 3. Sea surface heights observed by satellite Jason-1 (top), TOPEX/Poseidon (middle), and Envisat (bottom). The previous cycle data before the tsunami (gray crosses) were spatially filtered by the moving-average method with a bandwidth of 0.5 deg in latitude. Tsunami signals (open circles) have been extracted by subtracting the filtered data (black crosses) from the SSH data after the tsunami (gray triangles).

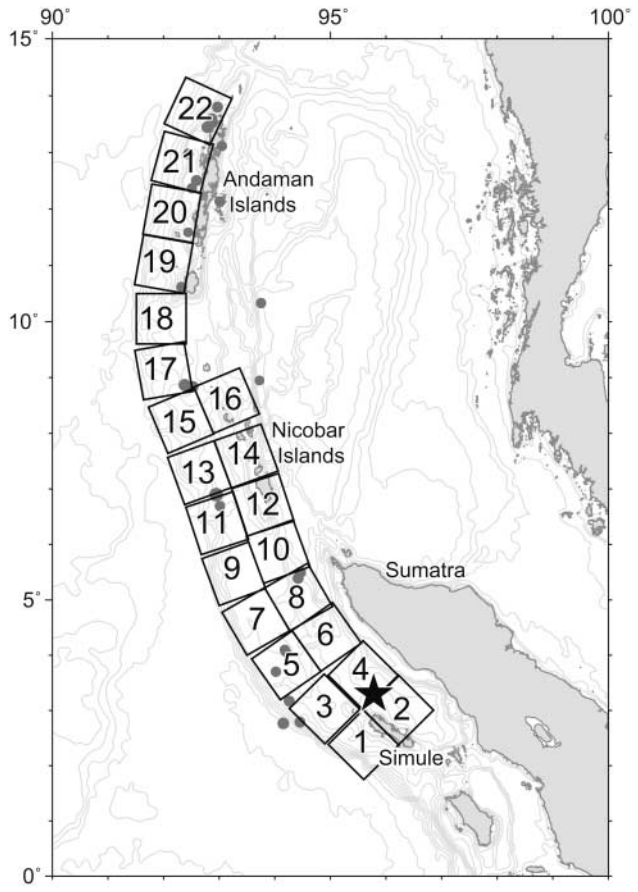

Figure 4. Subfault locations and numbers. Star shows the mainshock epicenter. Circles indicate aftershocks within one day after the mainshock.

for the tsunami numerical computation. For the global ocean, ETOPO2, the gridded bathymetry data derived from satellite altimetry observations or gravity data combined with shipboard echo-sounding measurements (Smith and Sandwell, 1997), is commonly used. However, ETOPO2 data are less reliable in the shallow ocean. To improve the accuracy, we have digitized nautical charts (United Kingdom Hydrographic Office, 2005) near coasts. The number of digitized chart sheets is 56 and the digitized ocean-depth points are 66,320, covering shallow coastal regions (Fig. 5). We merged these digitized depth points with the ETOPO2 data. In some shallow seas (e.g., Myanmar coast of Andaman Sea, Fig. 6), the original ETOPO2 data show deep (>100 m), canyonlike features, which do not appear in nautical charts.

Inversion

We assume that the observed tsunami waveforms or SSHs are linear superposition of tsunami waveforms, or Green's functions, computed from each subfault using the equations for coseismic displacement and the linear long-wave propagation. The slip amount on each subfault is estimated by inversion using the nonnegative least-squares method (Lawson and Hanson, 1974) to avoid negative slip. The errors for the solution are estimated by the delete-half-jackknife method, a resampling technique in which the inversion is repeated 100 times by randomly deleting a half of the data (waveforms and/or SSHs) to estimate the standard errors (e.g., Tichelaar and Ruff, 1989). We first used only tsunami waveform data on tide gauge stations, then SSH data of satellites. Finally, we carry out joint inversion of both datasets. The observed tsunami waveforms at tide gauges were resampled at a 1-min interval for the inversion. The total number of tsunami waveform data points used for the inversion is 708. We weighted Colombo data three times more than other tide gauge data, because we could use only the first peak. The total number of SSH data points used for inversion is 379, 87, and 584 for Jason-1, TOPEX/Poseidon,

and Envisat, respectively. The relative weights for tsunami waveforms to SSH data are therefore 708 to 1050. To quantitatively compare the results with different rupture velocities and rise times, we compute variance reduction of the observed and synthetic data (100% if they are identical).

Table 2
Subfault Parameters*

No.	Strike (°)	Dip (°)	Rake (°)	Lat† (° N)	Lon.† (° E)	Depth† (km)
1	315	10	95	1.75	95.60	3
2	315	10	95	2.38	96.23	20
3	315	10	95	2.40	94.90	3
4	315	10	95	3.00	95.60	20
5	325	10	100	3.20	94.10	3
6	325	10	100	3.71	94.83	20
7	330	10	105	4.00	93.50	3
8	330	10	105	4.44	94.27	20
9	340	10	105	4.90	93.00	3
10	340	10	105	5.30	93.80	20
11	342	10	100	5.82	92.68	3
12	342	10	100	6.15	93.50	20
13	340	10	95	6.72	92.38	3
14	340	10	95	7.02	93.22	20
15	337	10	85	7.64	92.08	3
16	337	10	85	8.00	92.90	20
17	350	10	99	8.60	91.64	3
18	0	10	106	9.60	91.51	3
19	10	10	115	10.66	91.48	3
20	10	10	115	11.56	91.63	3
21	15	10	120	12.51	91.78	3
22	25	10	130	13.51	92.01	3

*Length and width are 100 km for each subfault.
†Locations (latitude [Lat.], longitude [Lon.], and Depth) indicate the left bottom corner of each subfault.

Results

Inversion of Tide Gauge Data

Inversion of tsunami waveforms recorded on tide gauge stations yields a tsunami source length of about 900 km. The largest slip of 25 to 30 m is estimated on the southern and shallow part of the source region (subfaults 3 or 5), off the coast of Sumatra. Around the Nicobar Islands (subfaults 9

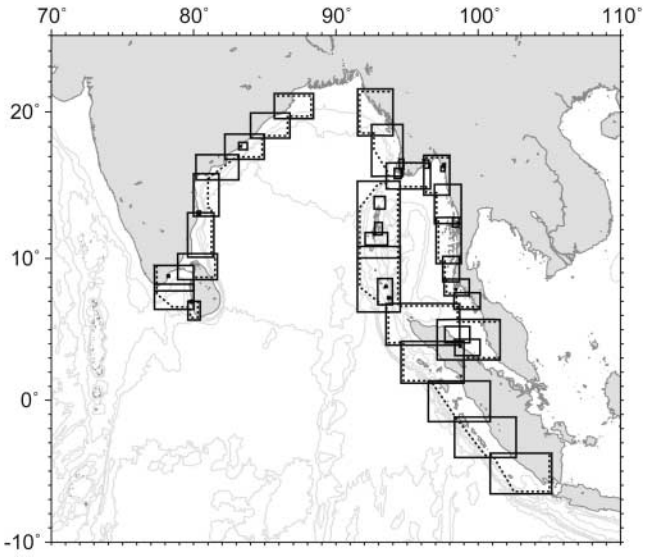

Figure 5. Distribution of digitized nautical charts (solid rectangular). We used digitized data for shallow regions bounded by dashed lines. For deeper parts, we used ETOPO2 data, merged with the digitized data if available.

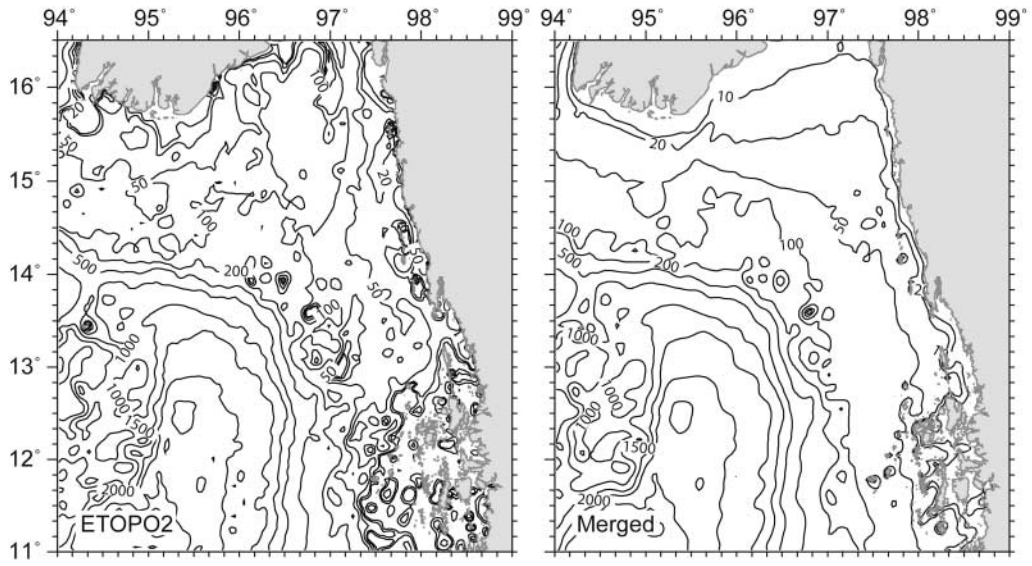

Figure 6. Comparison between ETOPO2 (left) and the merged bathymetry data (right).

to 16), the second largest region of slip up to 7 m is estimated. On the northern end of the source (subfaults 19 to 22) near the Andaman Islands, the estimated slip is relatively small (up to 2.5 m). This slip distribution is similar to those of Fine *et al.* (2005) and Tanioka *et al.* (2006).

These features are very stable, regardless of the rupture velocity or rise time chosen. The slip distribution for different rupture velocities (Fig. 7 and Table 3) shows that the largest slip on subfault 3 differs from 21 to 30 m, but large slip stays on the same subfaults. The general pattern of slip

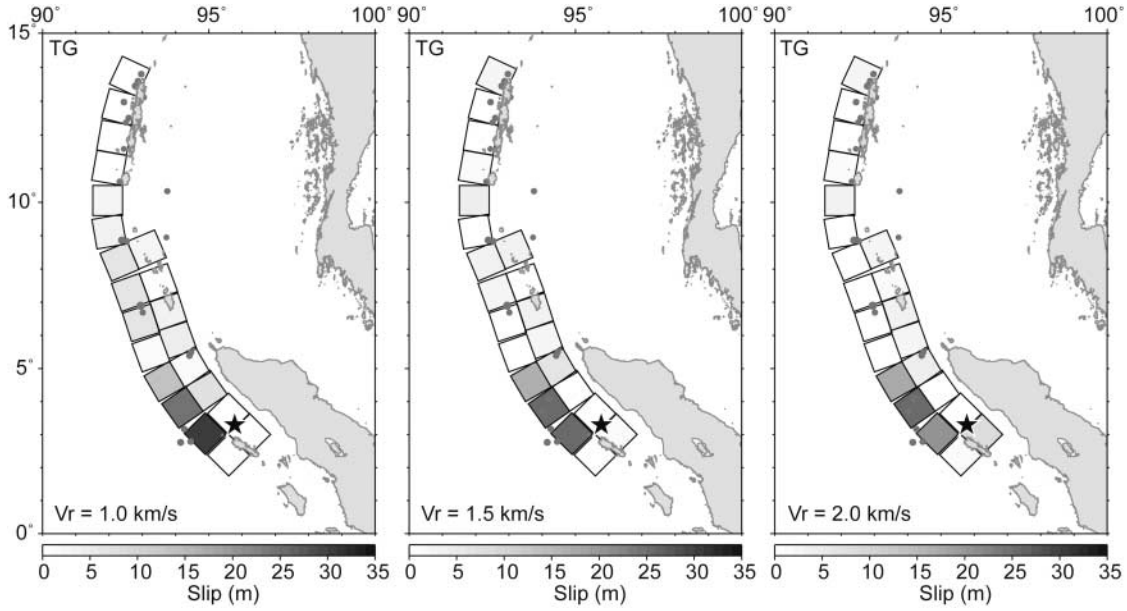

Figure 7. Slip distribution estimated by inversion of tide gauge (TG) data. Rupture velocity is 1.0 (left), 1.5 (center) and 2.0 (right) km/sec. Rise time for each subfault is 3 min.

Table 3
Slip Distributions for Three Different Inversions with Different Rupture Velocities

	Tide Gauge Data			Satellite Altimeter Data			TG + SA Data		
No.	1.0 km/sec	1.5 km/sec	2.0 km/sec	1.0 km/sec	1.5 km/sec	2.0 km/sec	1.0 km/sec	1.5 km/sec	2.0 km/sec
1	0.0 ± 0.2	0.0 ± 1.3	1.1 ± 10.5	10.4 ± 4.9	10.4 ± 5.0	8.0 ± 4.2	0.0 ± 0.2	0.0 ± 0.4	0.0 ± 1.4
2	0.0 ± 0.3	1.9 ± 1.2	8.5 ± 4.5	0.0 ± 1.7	0.0 ± 0.0	0.0 ± 0.0	4.3 ± 2.2	15.8 ± 7.8	19.6 ± 16.6
3	30.3 ± 15.5	25.4 ± 11.6	20.8 ± 9.2	1.0 ± 0.6	1.2 ± 0.6	3.6 ± 1.6	24.6 ± 13.7	18.6 ± 10.3	16.4 ± 7.0
4	0.0 ± 0.0	0.0 ± 0.0	0.0 ± 0.0	2.5 ± 1.1	0.7 ± 0.3	1.3 ± 0.6	0.0 ± 0.0	0.0 ± 0.0	0.0 ± 0.0
5	24.6 ± 10.0	25.5 ± 11.0	25.4 ± 9.1	30.2 ± 13.7	27.4 ± 16.3	24.3 ± 12.6	24.6 ± 9.8	26.6 ± 11.5	25.5 ± 10.2
6	7.4 ± 3.5	0.6 ± 0.4	0.0 ± 1.0	30.2 ± 15.4	35.0 ± 16.5	32.2 ± 16.0	12.3 ± 5.5	7.1 ± 3.2	3.9 ± 3.8
7	13.2 ± 5.9	16.6 ± 6.3	17.5 ± 7.8	19.7 ± 15.7	15.8 ± 7.4	18.1 ± 13.1	12.8 ± 7.6	15.7 ± 7.0	16.8 ± 8.0
8	1.7 ± 1.4	6.8 ± 3.4	4.9 ± 2.3	0.5 ± 9.8	3.0 ± 7.1	6.4 ± 7.4	1.8 ± 2.8	6.0 ± 3.2	4.7 ± 2.3
9	1.6 ± 1.2	0.0 ± 0.3	0.7 ± 0.2	15.4 ± 6.6	18.1 ± 8.3	17.5 ± 6.7	1.9 ± 3.9	0.0 ± 0.4	0.8 ± 0.4
10	4.2 ± 1.8	2.4 ± 1.6	2.6 ± 1.4	8.0 ± 4.1	11.3 ± 4.8	11.5 ± 5.1	4.5 ± 2.0	3.0 ± 1.3	3.3 ± 1.7
11	6.2 ± 3.2	0.8 ± 0.8	0.0 ± 0.5	14.9 ± 6.6	8.7 ± 4.6	9.8 ± 4.6	6.0 ± 3.3	1.0 ± 1.1	0.0 ± 0.5
12	3.9 ± 4.1	3.3 ± 3.5	3.2 ± 3.6	0.0 ± 0.2	0.0 ± 1.0	0.7 ± 0.5	3.2 ± 3.7	3.2 ± 3.7	2.7 ± 3.4
13	6.6 ± 2.8	2.8 ± 2.1	0.0 ± 0.7	7.4 ± 3.5	7.2 ± 3.5	8.6 ± 4.3	6.5 ± 2.6	2.4 ± 1.1	0.0 ± 0.5
14	0.0 ± 0.2	0.8 ± 2.4	1.2 ± 2.1	0.0 ± 0.0	0.0 ± 0.5	0.0 ± 0.2	0.0 ± 0.0	0.1 ± 0.2	0.9 ± 2.2
15	6.5 ± 3.0	3.1 ± 3.3	0.0 ± 0.5	12.7 ± 5.7	5.7 ± 2.3	8.3 ± 3.6	7.1 ± 2.9	3.6 ± 1.2	0.2 ± 0.2
16	2.8 ± 2.2	3.5 ± 1.4	2.5 ± 1.7	8.0 ± 3.8	14.2 ± 6.4	16.2 ± 7.4	3.5 ± 3.5	4.1 ± 1.4	2.7 ± 1.6
17	3.0 ± 1.8	0.0 ± 0.3	0.0 ± 0.0	6.1 ± 3.1	12.4 ± 5.1	11.0 ± 4.7	3.2 ± 1.9	0.0 ± 0.0	0.0 ± 0.0
18	2.5 ± 1.5	4.2 ± 2.7	3.9 ± 2.0	0.0 ± 0.4	4.6 ± 2.5	5.2 ± 2.8	2.7 ± 1.9	4.3 ± 2.5	4.0 ± 2.2
19	0.1 ± 0.2	1.6 ± 1.1	1.8 ± 1.0	0.0 ± 0.4	0.0 ± 1.0	0.0 ± 0.0	0.0 ± 0.3	1.7 ± 1.0	1.8 ± 1.0
20	0.0 ± 0.7	0.0 ± 0.0	0.0 ± 0.0	10.4 ± 5.2	0.0 ± 0.7	0.0 ± 1.6	0.0 ± 0.3	0.0 ± 0.0	0.0 ± 0.0
21	0.0 ± 0.2	0.0 ± 0.1	0.0 ± 0.3	0.0 ± 0.6	0.0 ± 0.0	0.0 ± 0.3	0.0 ± 0.1	0.0 ± 0.1	0.0 ± 0.4
22	0.7 ± 0.3	2.2 ± 1.0	2.5 ± 1.2	13.3 ± 6.4	9.7 ± 5.0	7.1 ± 4.1	1.0 ± 0.4	2.3 ± 1.1	2.6 ± 1.3
M_w	9.1	9.1	9.1	9.3	9.2	9.3	9.1	9.1	9.1
VR (%)	34.2	29.8	29.7	38.2	35.5	34.2	32.1	27.8	27.4

TG, tide gauge; SA, satellite altimeter; M_w, moment magnitude; VR, variance reduction.

distribution around the Nicobar and Andaman Islands are also stable. The maximum variance reduction was obtained in the case for rupture velocity of 1.0 km/sec (Table 4). We also varied the rise time on subfault for 1, 2, and 3 min, and found that the rise time 3 min gave the largest variance reduction (Table 4). We therefore adopt the case with rupture velocity of 1.0 km/sec and rise time 3 min as the best solution and compute synthetic SSHs (Fig. 8) and tsunami waveforms (Fig. 9).

The synthetic waveforms in general agree well with the observed ones at most stations (Fig. 9). The Vishakhapatnam waveform can be reproduced better, if we weight this station more. The overall slip distribution, that is, much smaller slip in the Andaman Islands than around the Nicobar Islands and off the coast of Sumatra, is similar for such a case. On the contrary, it is difficult to reproduce the Paradip waveform simultaneously with the other stations, in particular, Chennai and Vishakhapatnam. Synthetic SSHs in general reproduce the observed SSHs, but details such as the second peak of the direct arrival around 3° S of the Jason-1 record are not reproduced (Fig. 8) by a model estimated from tide gauge data alone. The total seismic moment is calculated from this slip distribution as 5.77×10^{22} N m (M_w 9.1), assuming the rigidity of 5.0×10^{10} N/m^2.

Inversion of Satellite Altimeter Data

Inversion of satellite data yields somewhat different results than inversion of the tide gauge data does. The largest slip is over 30 m, located on subfault 6 (Fig. 10). This is also in the southern part of the source region, or off the coast of Sumatra, but at a deeper part of the fault, and the slip amount is larger. We confirm from numerical experiments that deeper slip is required to explain the second peak of SSH data. The slip amount around the Nicobar Islands (subfaults 9 through 16) is up to 18 m, but mostly on shallow subfaults. The notable difference is that there is significant slip around the Andaman Islands at the northernmost subfault when satellite data are used. This indicates that the tsunami source extended over the entire aftershock zone with a length of about 1400 km, as suggested by Hirata *et al.* (2006).

Table 4
Variance Reductions (%) for Three Different Inversions with Different Rupture Velocities and Rise Times

V_r	Tide Gauge Data			Satellite Altimeter Data			TG + SA Data		
(km/sec)	1 min	2 min	3 min	1 min	2 min	3 min	1 min	2 min	3 min
0.5	23.1	20.8	18.8	27.8	29.5	31.0	22.0	20.1	18.3
1.0	32.8	33.4	34.2	33.8	36.4	38.2	29.8	31.0	32.1
1.5	29.3	29.5	29.8	31.1	33.8	35.5	26.8	27.3	27.8
2.0	30.2	29.9	29.7	29.7	32.3	34.2	27.2	27.3	27.4
2.5	28.4	28.2	28.3	28.4	30.6	32.9	25.0	25.2	25.6
3.0	28.5	28.4	28.5	27.4	29.7	31.9	24.9	25.2	25.6

As in the case of inverting the tide gauge data (previous section), the preceding feature is stable for different rupture velocities and rise times. The largest slip amount is similar (30 to 35 m) and always on subfault 6 (Fig. 10). The slip amount on the northernmost subfault (subfault 22) varies from 7 to 13 m when rupture velocity is changed from 1.0 to 2.0 km/sec (Fig. 10 and Table 3), but all the cases require significant slip. Within the range we varied these parameters, we found that the rupture velocity of 1.0 km/sec and the rise time of 3 min yield the largest variance reduction (Table 4).

The synthetic SSHs agree very well with the observed ones, including the second peak around 3° S of the Jason-1 record (Fig. 11). The synthetic tsunami waveforms, on the contrary, do not reproduce the observed ones in some cases (Fig. 12). In particular, on the east coast of India (Vishakhapatnam and Chennai) the synthetic waveforms are much larger than the observed tsunami amplitudes on tide gauges. The synthetic waveform at Paradip has similar amplitude with the observed one, but the phases are different. These discrepancies may be the result of significant slip on the northernmost subfaults around the Andaman Islands. The total seismic moment for this slip distribution is calculated as 9.53×10^{22} N m (M_w 9.3), assuming the rigidity of 5.0×10^{10} N/m^2.

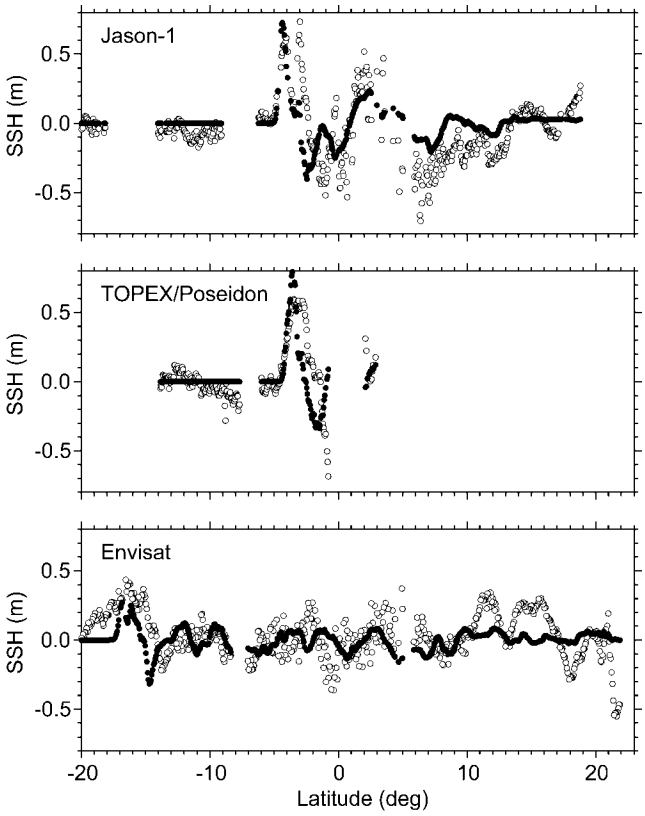

Figure 8. Comparison of observed (open circles) and synthetic (solid circles) SSHs computed from the slip distribution derived from inverting tide gauge data. Rupture velocity is 1.0 km/sec, but other rupture velocities yield similar results.

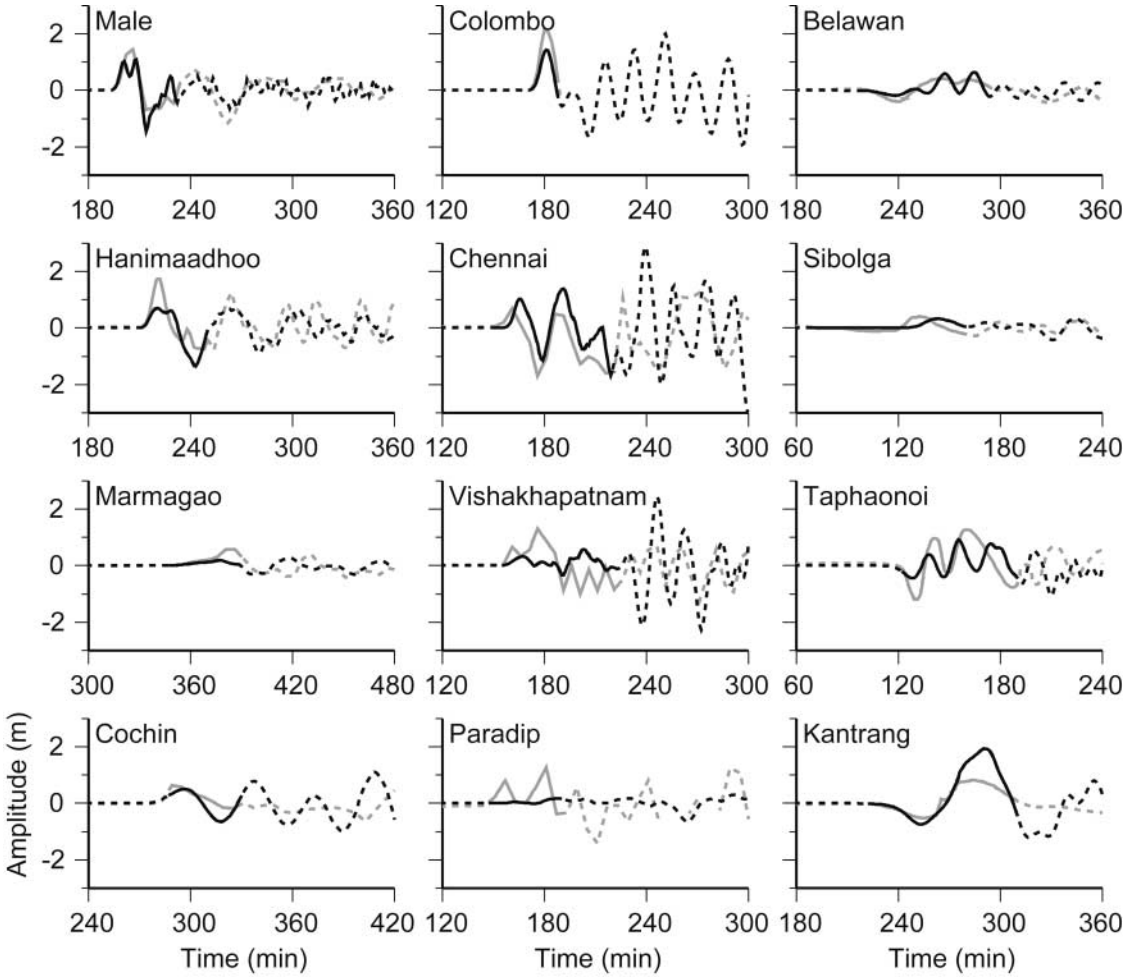

Figure 9. Comparison of observed (gray lines) and synthetic (black lines) tsunami waveforms computed from the slip distribution derived from inverting tide gauge data. Time ranges shown by solid curves are used for the inversion; the dashed parts are not used for the inversion, but shown for comparison. Rupture velocity is 1.0 km/sec.

Joint Inversion of Tide Gauge and Satellite Altimeter Data

Joint inversion of tide gauge and satellite data results in a slip distribution that is very similar to that of the tide gauge data (Fig. 13). Although the number of data points is larger, spatial and temporal distribution of SSH data is more limited than that of tide gauge data. The largest slip, about 25 m, is estimated on the southern and updip part of the source region off the coast of Sumatra. The slip on the northern subfaults, around the Andaman Islands, is relatively small, making the source about 900 km long.

Again, the previous slip distribution is stable for the choice of rupture velocity or rise time. The largest slip ranges 25 to 27 m on subfault 5 for different rupture velocities. The slip on subfault just north (subfault 7) and just south (subfault 3) on the updip part of the fault is also large, although the amount varies (13 to 25 m) depending on the rupture velocity (Fig. 13 and Table 3). For the subfaults around the Nicobar Islands, the slip is large on the shallow subfaults for a slower (1.0 km/sec) rupture velocity, whereas slip is greater on deeper subfaults for a faster (2.0 km/sec) rupture velocity. Slip on the northern subfaults (19 to 22) is almost zero for any rupture velocity. Comparison of the variance reduction indicates that the best fit between the observed and synthetic waveforms is obtained for a rupture velocity of 1.0 km/sec and a rise time of 3 min (Table 4). These are the critical parameters, therefore, although the resultant slip distribution is insensitive to the choice of rupture velocity and rise time.

Comparisons of the observed and synthetic sea surface heights (Fig. 14) indicate that the agreement is similar to the case of the tide gauge inversion (Fig. 8), that is, the second peak around 3° S of Jason-1 record was not reproduced. The observed and synthetic waveforms agree well at tide gauge stations (Fig. 15). The total seismic moment is 6.0×10^{22} N m (M_w 9.1) for the joint inversion, assuming the rigidity of 5.0×10^{10} N/m^2.

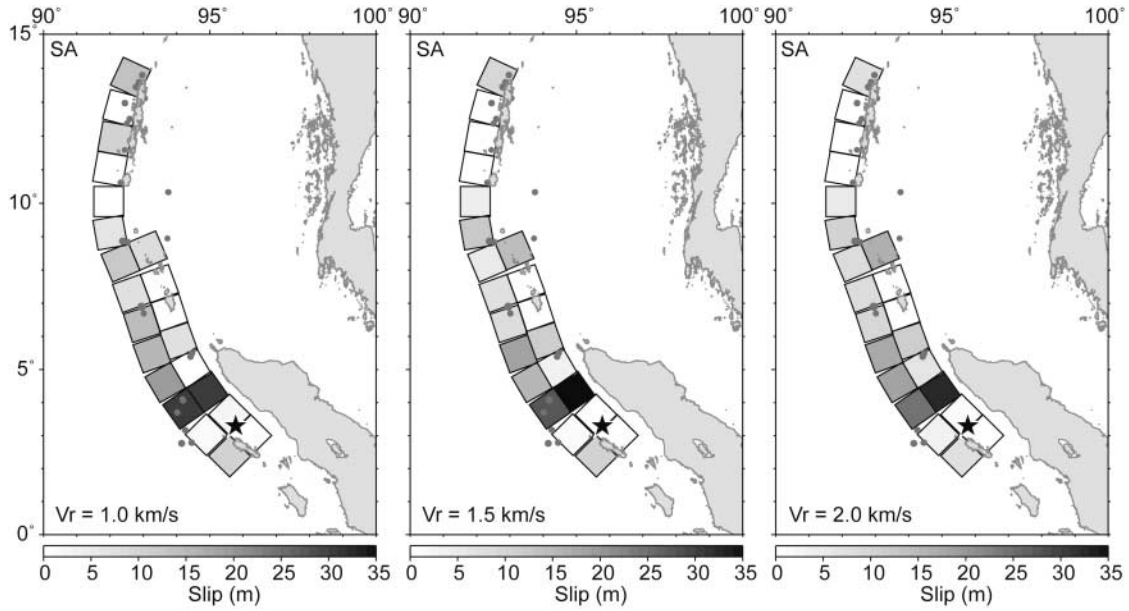

Figure 10. Slip distribution estimated by inversion of satellite altimeter (SA) data. Rupture velocity is 1.0 (left), 1.5 (center), and 2.0 (right) km/sec. Rise time for each subfault is 3 min.

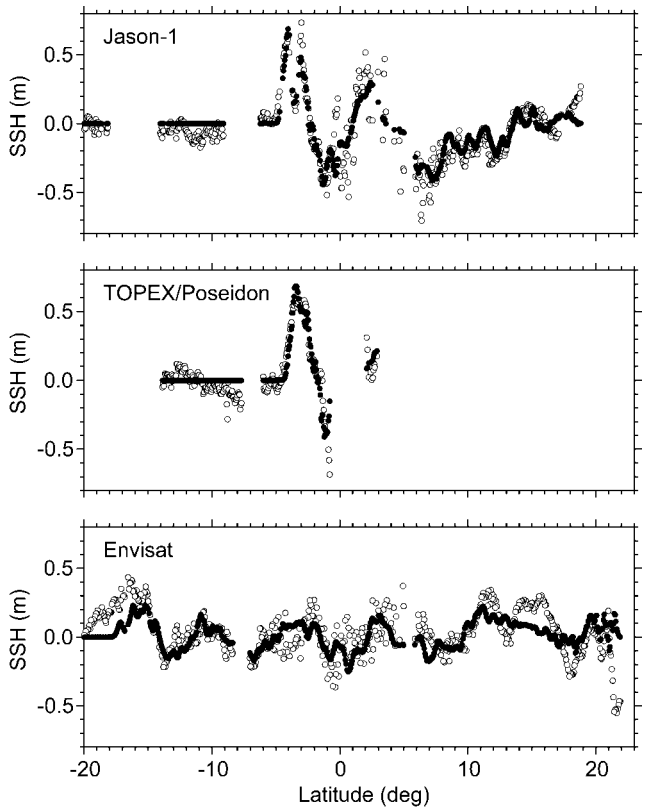

Figure 11. Comparison of observed (open circles) and synthetic (solid circles) SSHs computed from the slip distribution derived from inverting satellite altimeter data. Rupture velocity is 1.0 km/sec, but other rupture velocities yield similar results.

Discussion

Rupture Velocity

In seismic-source modeling, rupture velocity is one of the important parameters. In tsunami-source modeling, it is usually assumed that rupture is instantaneous for the entire fault, or that the rupture velocity is infinite. In the case of a giant earthquake whose source length is greater than several hundred kilometers, however, such an assumption may not be valid.

The previous studies of tsunami-source inversion using SSH data (Grilli *et al.*, 2005; Hirata *et al.*, 2006) suggested that a low rupture velocity of about 1.0 km/sec reproduces the observed SSH data. Our inversion of satellite data also indicates that the maximum variance reduction is obtained in case of low rupture velocity, 1.0 km/sec. We also note, however, that the comparisons of the observed and synthetic SSH data are quite similar in any case of rupture velocities; hence, the slower rupture velocity is not well resolved. The rupture velocity estimated from seismic-data analysis prefers the faster velocity over 2.5 km/sec (Ammon *et al.*, 2005; Ishii *et al.*, 2005).

We varied the rupture velocity and compared the synthetic tsunami waveforms for the slip distribution estimated by the joint inversion (Fig. 16). The synthetic waveforms are sensitive to the rupture velocities only at tide gauge stations in Sri Lanka and along the east coast of India. At Colombo and Chennai, the synthetic waveforms for a rupture velocity of 1.0 km best explain the observed waveforms. From this comparison, we suggest that a rupture velocity of 1.0 km/

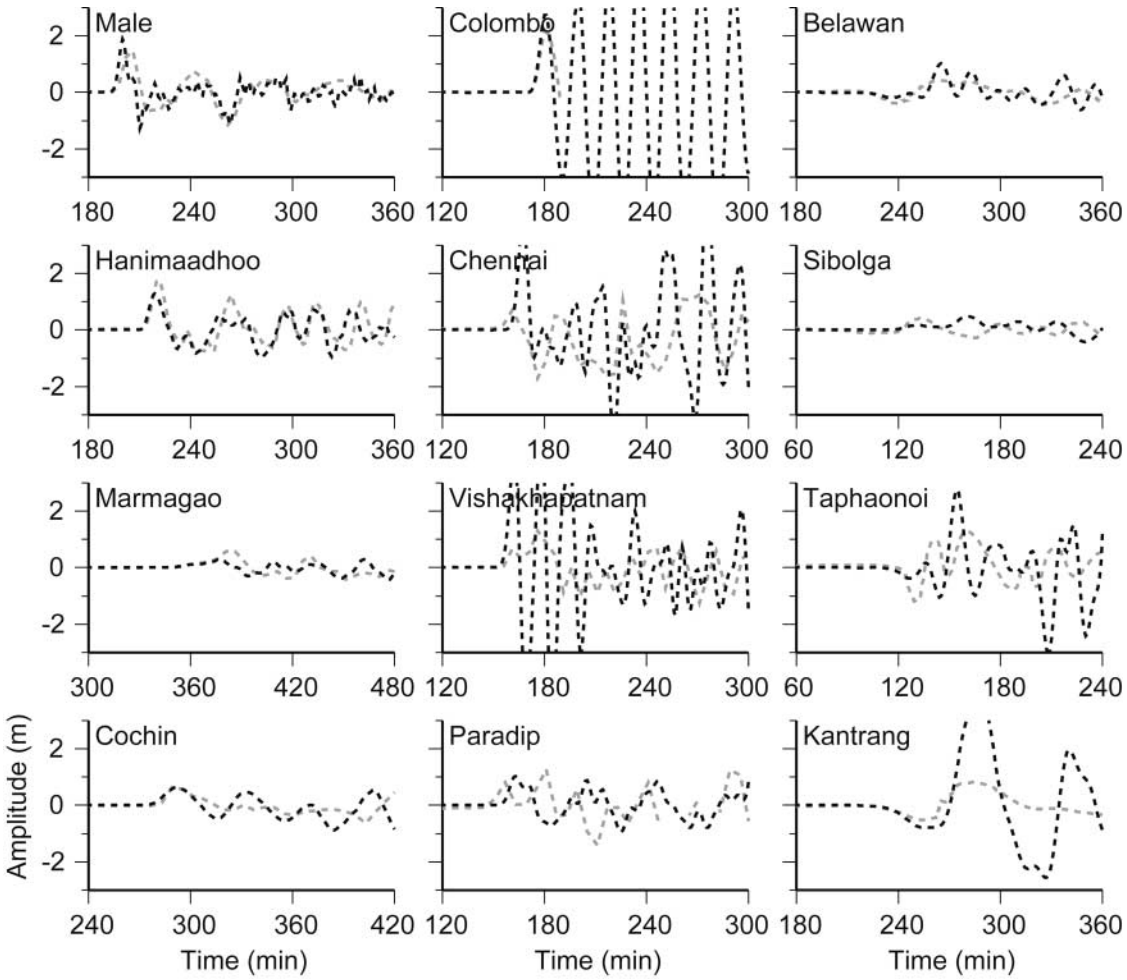

Figure 12. Comparison of observed (gray lines) and synthetic (black lines) tsunami waveforms computed from the slip distribution derived from inverting satellite altimeter data. Rupture velocity is 1.0 km/sec.

sec is preferred for the tsunami source. In this article, we assumed a uniform rupture velocity. As suggested by Lay *et al.* (2005b), the rupture velocity might have varied during the rupture process. Because waveforms are sensitive to rupture velocity only at a few tide gauge stations, the temporal change in rupture velocity may not be resolvable from tsunami data.

Slip Distribution and Crustal Deformation

Our inversion indicates that maximum slip is located off Sumatra Island. This is similar to the result of analyses using seismic waveforms (Ammon *et al.*, 2005). The moderate slip around the Nicobar Islands is also similar to their result. Around the Andaman Islands, our inversion of tide gauge data and the joint inversion indicate little slip, whereas our inversion of satellite data indicates significant slip there. Spatial distribution of coastal subsidence and uplift has been revealed from comparisons of satellite imagery before and after the earthquake (Meltzner *et al.*, 2006; Tobita *et al.*, 2006). Seafloor deformation calculated from the three models (Fig. 17) shows large (up to 14 m) uplift of the seafloor in the southern part of the source. The large seafloor uplift there must be responsible for the large tsunami damage in and around Banda Aceh. Our results predict uplift near the trench axis and subsidence of the Nicobar Islands. However, the subsidence amount predicted by tsunami source model is up to 1.2 m, too small compared with the observed subsidence, up to 3 m on Great Nicobar Island (e.g., Malik and Murty, 2005). Our joint inversion (right figure in Fig. 17) predicts little deformation on the Andaman Islands, whereas the inversion of only satellite data predicts some deformation. The field surveys indicate that North and Middle Andaman Islands have uplifted as much as 1.5 m whereas South Andaman has subsided nearly 1 m (Kayanne *et al.*, 2005).

If the tsunami data do not support the slip beneath the Andaman Islands, the observed sea level changes must be produced by a slow slip at a timescale longer than tsunami periods or postseismic slip after tsunami generation but before the survey.

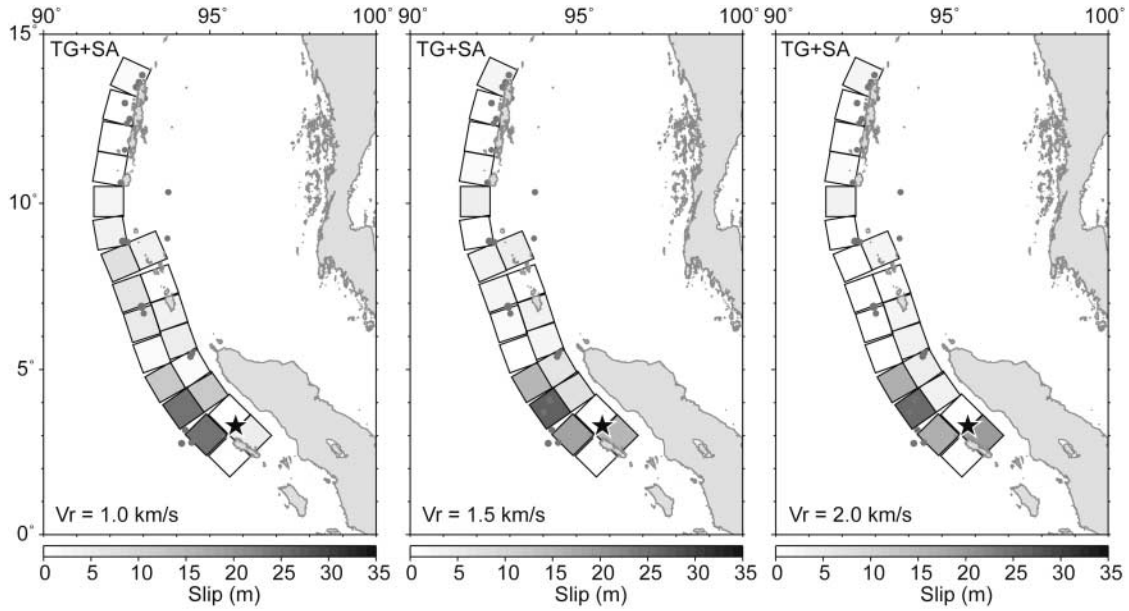

Figure 13. Slip distribution estimated by joint inversion of tide gauge and satellite altimeter (TG + SA) data. Rupture velocity is 1.0 (left), 1.5 (center), and 2.0 (right) km/sec. Rise time for each subfault is 3 min.

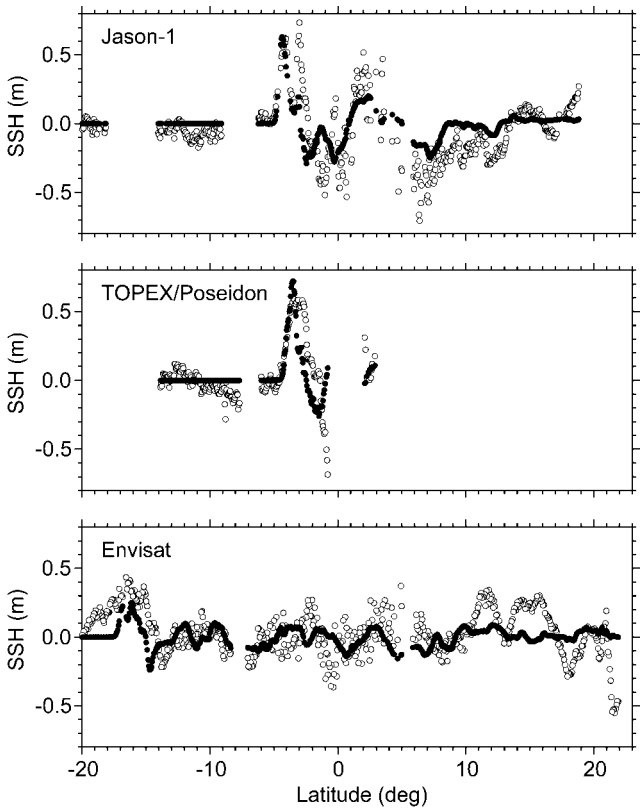

Figure 14. Comparison of observed (open circles) and synthetic (solid circles) SSHs computed from the slip distribution derived from joint inversion of tide gauge and satellite altimeter data. Rupture velocity is 1.0 km/sec.

Slip near the Andaman Islands

Slip around the Andaman Islands is an important key to estimate the tsunami source length. To assess the effect of the slip around the Andaman Islands on the synthetic tsunami waveforms, we compare the observed tsunami waveforms on the east coast of India and Sri Lanka with the synthetic waveforms computed from three models (Fig. 18). The slip distribution estimated by inversion of satellite data, which has a considerable slip around the Andaman Islands, does not explain the observed tsunami waveforms. The amplitudes at Vishakhapatnam and Chennai are overestimated from the initial pulse to the later phases of tsunamis. In contrast, the synthetic waveforms computed from the slip distribution derived from the joint inversion, with a little slip in the Andaman Islands, can reproduce the observed tsunami waveforms at those tide gauges. This suggests that the tide gauge data do not support slip around the Andaman Islands. The fact that the tsunami height and damage were slight in Myanmar, compared with the neighboring Thai coast, also is consistent with a source limited in the southern part of the aftershock zone (Satake *et al.*, 2006).

Conclusion

We have estimated the tsunami source of the 2004 Sumatra–Andaman earthquake using tsunami waveforms at tide gauge stations and SSHs captured by satellite altimetry measurements over the Indian Ocean. Joint inversion of tsunami waveforms and satellite data indicates that the 2004 tsunami source was about 900 km long, extending from off

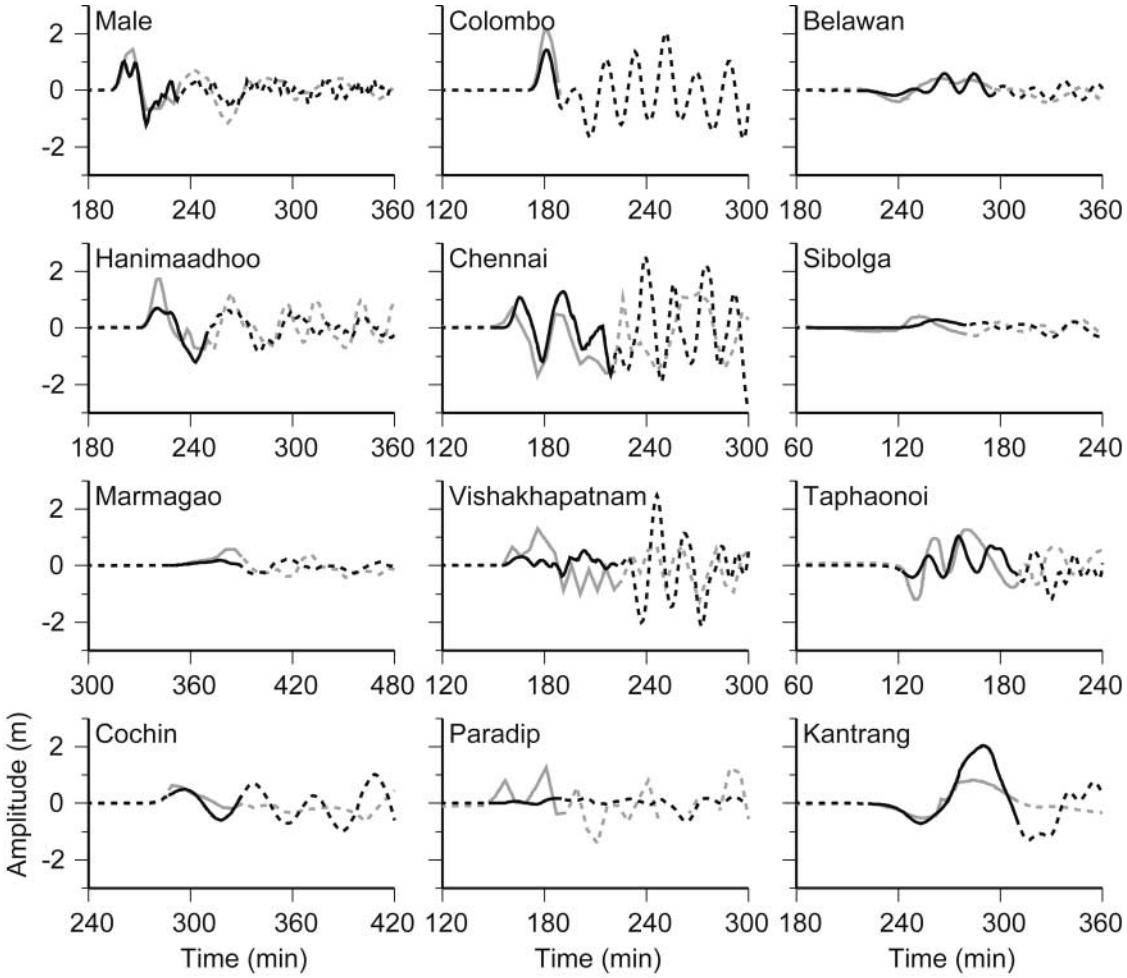

Figure 15. Comparison of observed (gray lines) and the synthetic (black lines) tsunami waveforms computed from the slip distribution derived from joint inversion of tide gauge and satellite altimeter data. Time ranges shown by solid curves are used for the inversion; the dashed parts are not used for the inversion, but shown for comparison. Rupture velocity is 1.0 km/sec.

the west coast of Sumatra (maximum region of slip) to the Nicobar Islands. Slip on the fault is 13 to 25 m off Sumatra, up to 7 m around the Nicobar Islands, and relatively little farther north around the Andaman Islands. The agreement between observed and synthetic waveforms is best using a rupture velocity of 1.0 km/sec and a rise time on each subfault of 3 min.

Acknowledgments

We appreciate N. Sato for her tough job of digitizing several nautical charts. We thank Survey of India and National Institute of Oceanography, Y. Tanioka and H. Matsumoto for providing us tide gauge data of India, Indonesia, and Thailand, respectively. We thank S. Bilek, E. Geist, D. Shankar, A. Rabinovich, M. Chlieh, M. Leonard, and K. Hirata for their valuable comments to improve our manuscript. Most of the figures were generated by using Generic Mapping Tools (Wessel and Smith, 1998).

References

Ammon, C. J., C. Ji, H. K. Thio, D. Robinson, S. D. Ni, V. Hjorleifsdottir, H. Kanamori, T. Lay, S. Das, D. Helmberger, G. Ichinose, J. Polet, and D. Wald (2005). Rupture process of the 2004 Sumatra-Andaman earthquake, *Science* **308,** 1133–1139.

Araki, E., M. Shinohara, K. Obana, Y. Kaneda, T. Kanazawa, and K. Suyehiro (2006). Aftershock distribution of December 26, 2004 off-Sumatra earthquake from ocean bottom seismographic observation, *Earth Planets Space* **58,** 113–119.

Fine, I. V., A. B. Rabinovich, and R. E. Thomson (2005). The dual source region for the 2004 Sumatra tsunami, *Geophys. Res. Lett.* **32,** L16602, doi 10.1029/2005GL023521.

Global Centroid Moment Tensor (CMT) Project catalog search, www.globalcmt.org/CMTsearch.html (last accessed May 2005).

Gower, J. (2005). Jason 1 detects the 26 December 2004 tsunami, *EOS Trans. AGU* **86,** 37–38.

Grilli, S. T., M. Ioualalen, J. Asavanant, J. T. Kirby, F. Shi, P. Watts, and F. Dias (2005). Modeling of the 12/26/04 Indian Ocean Tsunami generation, propagation, and coastal impact. Integration of SEATOS

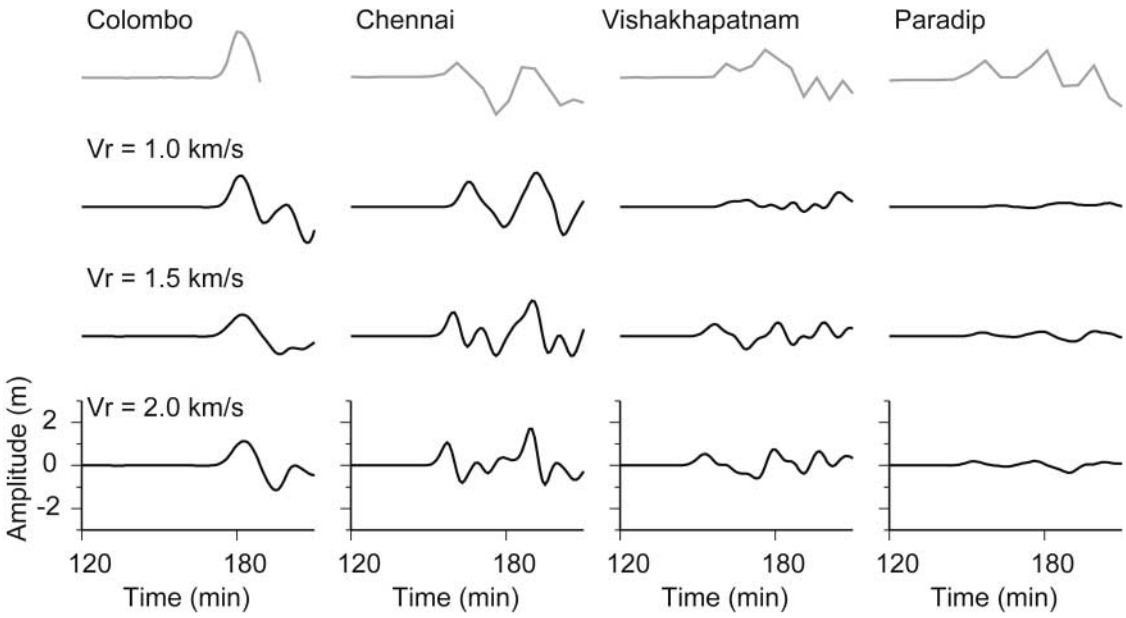

Figure 16. Comparison of observed (gray) and synthetic (lower rows) tsunami waveforms resulting from three rupture velocities of 1.0, 1.5, and 2.0 km/sec. Rise time for each subfault is 3 min.

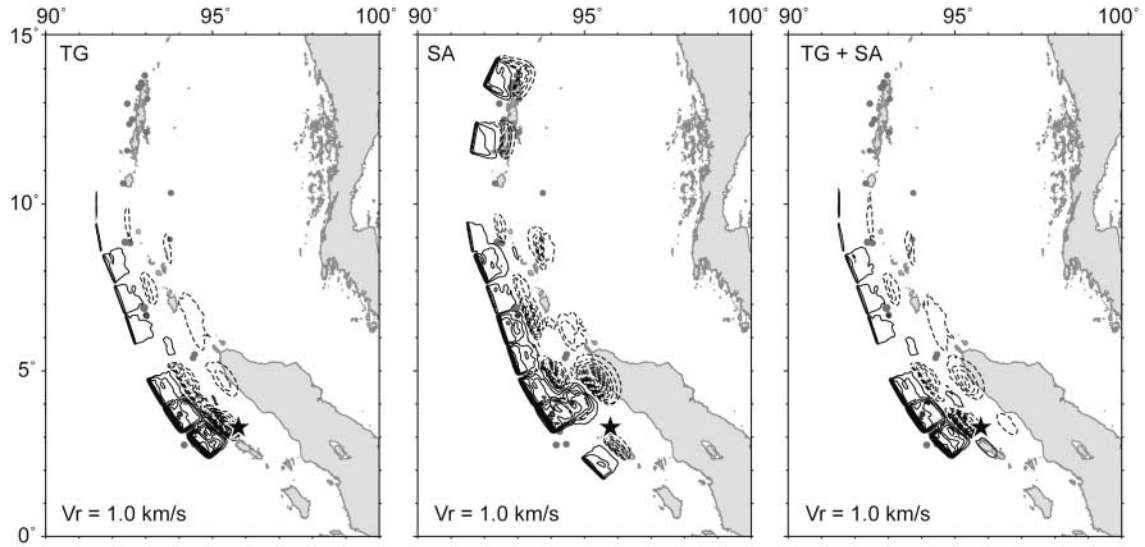

Figure 17. Crustal deformations computed from the slip distribution estimated by tide gauge data (left), satellite altimeter data (center), and the joint inversion of tide gauge and satellite altimeter data (right). The solid contours indicate uplift with the contour interval of 1.0 m, whereas the dashed contours indicate subsidence with the contour interval of 0.5 m.

Cruise and other geophysical data (abstract), *EOS Trans. AGU* **86,** (Fall Meet. Suppl.), U13A-07.

Hirata, K., K. Satake, Y. Tanioka, T. Kuragano, Y. Hasegawa, Y. Hayashi, and N. Hamada (2006). The 2004 Indian Ocean tsunami: Tsunami source model from satellite altimetry, *Earth Planets Space* **58,** 195–201.

International Federation of Red Cross and Red Crescent Societies (2005). *World Disasters Report*, Kumarian Press, Bloomfield, Connecticut, 246 pp.

Ishii, M., P. M. Shearer, H. Houston, and J. E. Vidale (2005). Extent, duration and speed of the 2004 Sumatra-Andaman earthquake imaged by the Hi-Net array, *Nature* **435,** 933–936.

Kayanne, H., Y. Ikeda, T. Echigo, M. Shishikura, and T. Kamataki (2005). Coseismic uplift of the Andaman Islands associated with the Sumatra-Andaman Earthquake of 2004 and the recurrence history of gigantic earthquakes, in *Memorial Conference on the 2004 Giant Earthquake and Tsunami in the Indian Ocean, Programs and Abstracts*, P1-2-1-2.

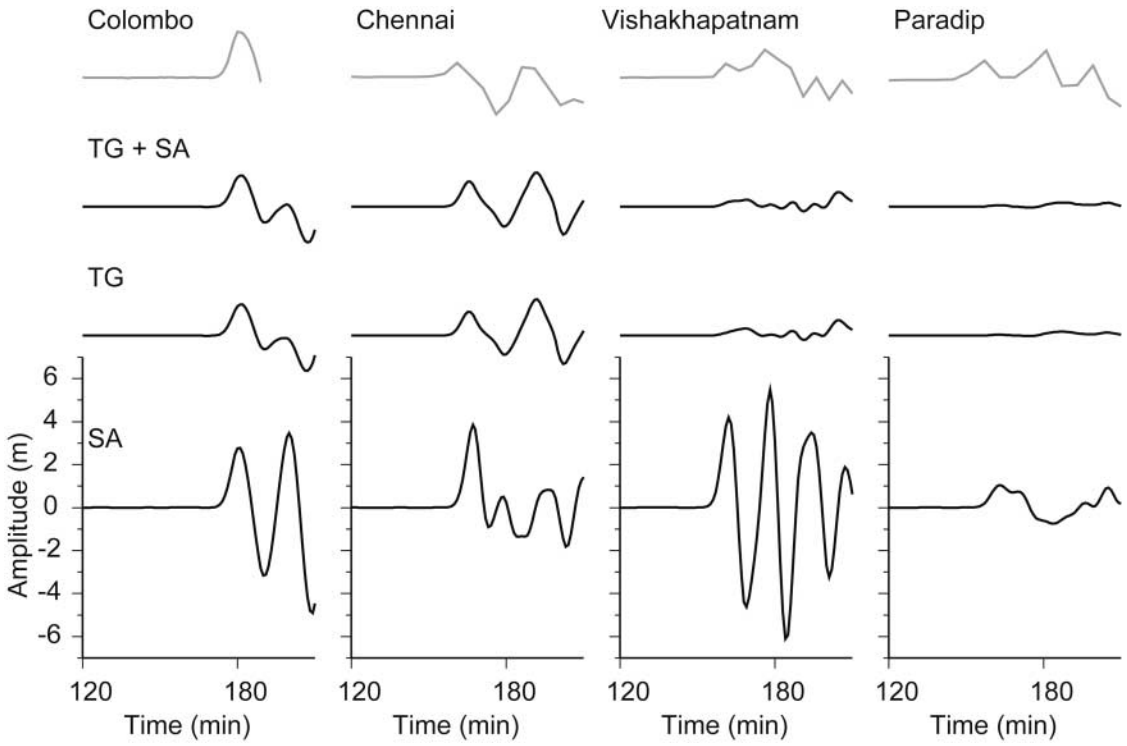

Figure 18. Comparison of observed (top) and synthetic tsunami waveforms computed from a joint inversion of tide gauge and satellite data (top middle), inversion of tide gauge data (middle bottom), and satellite altimeter data (bottom). Note that the slip distribution estimated by satellite altimeter data has significant slip in the northernmost subfaults around the Andaman Islands.

Lawson, C. L., and R. J. Hanson (1974). *Solving Least Squares Problems*, Prentice Hall, Inc., Englewood Cliffs, New Jersey, 340 pp.

Lay, T., H. Kanamori, C. J. Ammon, M. Nettles, S. N. Ward, R. C. Aster, S. L. Beck, S. L. Bilek, M. R. Brudzinski, R. Butler, H. R. DeShon, G. Ekstrom, K. Satake, and S. Sipkin (2005a). The great Sumatra-Andaman earthquake of 26 December 2004, *Science* **308,** 1127–1133.

Lay, T., H. Kanamori, C. J. Ammon, M. Nettles, S. N. Ward, R. Aster, S. L. Beck, S. L. Bilek, M. R. Brudzinski, R. Butler, H. R. DeShon, G. Ekstrom, K. Satake, and S. Sipkin (2005b). Response to "Comment on 'The great Sumatra-Andaman earthquake of 26 December 2004,'" by S. Neetu, I. Suresh, R. Shankar, D. Shankar, S. S. C. Shenoi, S. R. Shetye, D. Sundar, and B. Nagarajan, *Science* **310,** 1431.

Malik, J. N., and C. V. R. Murty (2005). Landscape changes in Andaman and Nicobar Islands (India) due to Mw 9.3 tsunamigenic Sumatra earthquake of 26 December 2004, *Curr. Sci.* **88,** 1384–1386.

Meltzner, A. J., K. Sieh, M. Abrams, D. C. Agnew, K. W. Hudnut, J.-P. Avouac, and D. H. Natawidjaja (2006). Uplift and subsidence associated with the great Aceh-Andaman earthquake of 2004, *J. Geophys. Res.* **111,** B02407, doi 10.1029/2005JB003891.

Merrifield, M. A., Y. L. Firing, T. Aarup, W. Agricole, G. Brundrit, D. Chang-Seng, R. Farre, B. Kilonsky, W. Knight, L. Kong, C. Magori, P. Manurung, C. McCreery, W. Mitchell, S. Pillay, F. Schindele, F. Shillington, L. Testut, E. M. S. Wijeratne, P. Caldwell, J. Jardin, S. Nakahara, F. Y. Porter, and N. Turetsky (2005). Tide gauge observations of the Indian Ocean tsunami, December 26, 2004, *Geophys. Res. Lett.* **32,** L09603, doi 10.1029/2005GL022610.

Nagarajan, B., I. Suresh, D. Sundar, R. Sharma, A. K. Lal, S. Neetu, S. S. C. Shenoi, S. R. Shetye, and D. Shankar (2006). The Great Tsunami of 26 December 2004: A description based on tide-gauge data from the Indian subcontinent and surrounding areas, *Earth Planets Space* **58,** 211–215.

Neetu, S., I. Suresh, R. Shankar, D. Shankar, S. S. C. Shenoi, S. R. Shetye, D. Sundar, and B. Nagarajan (2005). Comment on "The great Sumatra-Andaman earthquake of 26 December 2004" by T. Lay, H. Kanamori, C. J. Ammon, M. Nettles, S. N. Ward, R. C. Aster, S. L. Beck, S. L. Bilek, M. R. Brudzinski, R. Butler, H. R. DeShon, G. Ekstrom, K. Satake, and S. Sipkin, *Science* **310,** 1431.

Okada, Y. (1985). Surface deformation due to shear and tensile faults in a half-space, *Bull. Seism. Soc. Am.* **75,** 1135–1154.

Park, J., T. R. A. Song, J. Tromp, E. Okal, S. Stein, G. Roult, E. Clevede, G. Laske, H. Kanamori, P. Davis, J. Berger, C. Braitenberg, M. Van Camp, X. Lei, H. P. Sun, H. Z. Xu, and S. Rosat (2005). Earth's free oscillations excited by the 26 December 2004 Sumatra-Andaman earthquake, *Science* **308,** 1139–1144.

Piatanesi, A., and S. Lorito (2007). Rupture prosess of the 2004 Sumatra-Andaman earthquake from tsunami waveform inversion, *Bull. Seism. Soc. Am.* **97,** no. 1A, S223–S231.

Satake, K. (1995). Linear and Nonlinear Computations of the 1992 Nicaragua earthquake tsunami, *Pure Appl. Geophys.* **144,** 455–470.

Satake, K., T. T. Aung, Y. Sawai, Y. Okamura, K. S. Win, W. Swe, C. Swe, T. L. Swe, S. T. Tun, M. M. Soe, T. Z. Oo, and S. H. Zaw (2006). Tsunami heights and damage along the Myanmar coast from the December 2004 Sumatra-Andaman earthquake, *Earth Planets Space* **58,** 243–252.

Singh, S. K., M. Ortiz, H. K. Gupta, and D. G. A. Ramadass (2006). Slow Slip below Port Blair, Andaman during the Great Sumatra-Andaman Earthquake of 26 December, 2004, *Geophys. Res. Lett.* **33,** doi 10.1029/2005GL025025.

Smith, W. H. F., and D. T. Sandwell (1997). Global sea floor topography from satellite altimetry and ship depth soundings, *Science* **277,** 1956–1962.

Stein, S., and E. A. Okal (2005). Speed and size of the Sumatra earthquake, *Nature* **434,** 581–582.

Tanioka, Y., and K. Satake (1996). Tsunami generation by horizontal displacement of ocean bottom, *Geophys. Res. Lett.* **23,** 861–864.

Tanioka, Y., Y. Yudhicara, T. Kususose, S. Kathiroli, Y. Nishimura, S. I. Iwasaki, and K. Satake (2006). Rupture process of the 2004 great Sumatra-Andaman earthquake estimated from tsunami waveforms, *Earth Planets Space* **58,** 203–209.

Tichelaar, B. W., and L. J. Ruff (1989). How good are our best models? Jackknifing, Bootstrapping, and earthquake depth, *EOS Trans. AGU* **70,** 593, 605–606.

Tobita, M., H. Suito, T. Imakiire, M. Kato, S. Fujiwara, and M. Murakami (2006). Outline of vertical displacement of the 2004 and 2005 Sumatra earthquakes revealed by satellite radar imagery, *Earth Planets Space* **58,** e1–e4.

Tsuji, Y., Y. Namegaya, H. Matsumoto, S.-I. Iwasaki, W. Kanbua, M. Sriwichai, and V. Meesuk (2006). The 2004 Indian tsunami in Thailand: tsunami height and tide gauge records, *Earth Planets Space* **58,** 223–232.

United Kingdom Hydrographic Office (2005). Catalogue of Admiralty Charts and Publications, 2005 Edition, Taunton, Somerset, United Kingdom.

Wessel, P., and W. H. F. Smith (1998). New, improved version of the Generic Mapping Tools released, *EOS Trans. AGU* **79,** 579.

Geological Survey of Japan (GSJ)
National Institute of Advanced Industrial Science and Technology (AIST)
Tsukuba Central 7, 1-1-1 Higashi, Tsukuba
Ibaraki 305-8567, Japan

Manuscript received 13 January 2006.